RSC Advances

ROYAL SOCIETY OF CHEMISTRY

www.rsc.org/advances

Cite this: DOI: 10.1039/c0xx00000x

www.rsc.org/catalysis

Article

Remarkable crystal phase effect of Cu/TiO_2 catalysts on the selective hydrogenation of dimethyl oxalate

Bin Wang, Chao Wen, Yuanyuan Cui, Xi Chen, Yu Dong, and Wei-Lin Dai

Received (in XXX, XXX) XthXXXXXXXXX 201X, Accepted Xth XXXXXXXXX 201X
DOI: 10.1039/b000000x

A series of Cu based TiO_2 supported catalysts were synthesized via facile ammonia evaporation for the selective hydrogenation of dimethyl oxalate (DMO) to ethylene glycol (EG). It is found that 100% conversion of DMO and 99% selectivity to EG as well as super stability could be achieved over the 20% Cu/P25 catalyst. The effect of crystal phase of titania support as well as the interaction between Cu and P25 were investigated. Active copper species located at the interface between anatase and rutile play important roles in the selective hydrogenation. The excellent catalytic performance was mainly attributed to a better copper dispersion and an appropriate ratio of Cu^0/Cu^+, which stem from an intimate interaction between Cu and P25 support.

1. Introduction

With the soaring demand in petroleum-related derivatives and increasing shortage of oil resources, an alternative for these products is urgently hankered. Recently, a catalytic process of coal-to-ethylene glycol (CTE) has entranced numerous attention for the broad application of ethylene glycol (EG) such as antifreeze, coolant, polyester and solvents, *etc*.[1] and also for the environmental friendliness and lower cost of the reaction routine, because the CTE process is superior to the traditional ethylene oxide's hydration route.

As is known, the booming CTE approach comprises two steps: first, coupling of CO with nitrite esters to obtain dimethyl oxalate (DMO), whose industrial scale has achieved 10,000 tons per year in 2010,[2] and then the sequential hydrogenation of DMO to the desired products, which is now the very focus of academic and industrial research.

Tremendous work has been conducted to investigate various catalysts from the viewpoint of texture, structure, catalytic activity and stability. Previous researches revealed that copper-based catalysts exerted excellent catalytic activities as well as longer stability,[3-7] especially for the silica supported ones.[8-10] Chen *et al.*[8] explored the influence of ammonia-evaporation (AE) temperature and cooperative effect between Cu^0 and Cu^+ in the catalytic results. Yin *et al*. introduced hexagonal mesoporous silica (HMS) as a novel support, thus significantly promoting the catalytic performances.[9] Thereafter, various catalysts have been synthesized with HMS support.[10-14] Unfortunately, the catalyst tends to deactivate for its easy erosion of SiO_2 support, along with the aggregation of copper species under elevated reaction temperatures.[2,6] Taken these into consideration, it is of significance to devise a catalyst that supported on non-silicon matrix.

Titania, a versatile material in photocatalytic, gas-sensing and heterogeneous reactions,[15-17] had found an increasingly wide application in catalytic systems. Numerous investigations has been dedicated to exploit the interaction between active species and TiO_2 matrix, particularly the P25 TiO_2, a universal titania that comprise around 80% anatase and 20% rutile by weight. Xia *et al.*[18] achieved ultrahigh stability in $Pt/CNT@TiO_2$ and assigned that to strong metal-support interaction between Pt and TiO_2 based support. Analogous metal-support interaction were observed in Jiang's and Kou's groups.[19,20] Jovic *et al.*[21] gauged the electron transfer between the anatase and rutile interface of the Au/P25 TiO_2 in the H_2 production from ethanol. The intimate contact was discovered among anatase, rutile and Au particles, which should take responsibility for the high catalytic performance. Murdoch and coworkers observed a marked difference in H_2 production rate on Au/TiO_2 anatase and Au/TiO_2 rutile,[22] which was attributed to variations in electron-hole recombination rates. Similar results were also inspected by several other groups.[23-25] Besides, much work have revealed that moderate surface and textural properties may induce a strong metal support interaction (SMSI).[26-27]

Ground upon the above advantages, it is highly expected that titania support should play a part in an even wider range of chemistry, one aspect to name, catalysis. However, to the best of our knowledge, in spite of the intimate interaction between metal and TiO_2 support, no study regarding the performance of Cu/TiO_2 in the vapor-phase hydrogenation of DMO to EG has been reported. Herein, we report a Cu/TiO_2 catalytic system with perfect catalytic performance, and investigate the support morphology with various characterization methods and expect that would shed some light on the future exploration in titania-supported heterogeneous systems.

2. Experimental

2.1 Catalyst preparation

All the reagents are purchased from Sinopharm Chemical Reagent Co., Ltd. without further purification, unless otherwise specified.

The Cu/P25 TiO_2 (Degussa Co., Ltd) catalyst precursor with different morphology of support is prepared by AE method.[8] Firstly, 6.1 g of $Cu(NO_3)_2{\cdot}3H_2O$ were dissolved into 200 mL of

deionized water, and then about 23 mL of aqueous ammonia (25 wt.%) were added and stirred for 0.5 h at 333 K. The initial pH of the suspension was 11-12. After that, 6.4 g of P25 TiO_2 were added to the above solution and stirred for another 4 h. The suspension was then preheated at 363 K to allow for the evaporation of ammonia and the decrease of pH as well as the consequent deposition of copper species on titania. When the pH value of the suspension was decreased to 6-7, the evaporation process was terminated. The residue was washed with deionized water three times and ethanol once followed by drying at 393 K overnight. The catalyst precursors were calcined at a 823 K for 4 h, pelletized, crushed, sieved to 40-60 meshes, and denoted as 20CuP25-823 (simplified as Cu/P25), where 20 and 823 signify the copper mass concentration and calcination temperature.

For comparison, the copper-based catalysts supported on pure anatase TiO_2 (Aladdin Co., Ltd), pure rutile TiO_2 (Aladdin Co., Ltd), and TiO_2 that was mechanically mixed with A and R (A/R=80:20) denoted as 20Cu/A-823, 20Cu/R-823 and 20Cu/M-823 (simplified as Cu/A, Cu/R and Cu/M), respectively, were also prepared by the AE method.

2.2 Catalyst characterization

The BET surface area (S_{BET}) was measured using N_2 physisorption at 77 K on a Micromeritics Tristar 3000 apparatus. The pore size distributions were obtained from the desorption isotherm branch of the nitrogen isotherms using Barrett-Joyner-Halenda (BJH) method.

The wide-angle XRD patterns were collected on a Bruker D8 Advance X-ray diffractometer using nickel-filtered Cu Kα radiation (λ= 0.15406 nm) with a scanning angle (2θ) of 20-80°, a scanning speed of 4°·min^{-1}, and a voltage and current of 40 kV and 40 mA, respectively.

TEM characterization was performed on a JEOL JEM 2010 instrument. Samples for electron microscopy observation are prepared by grinding and subsequent dispersing the powder in ethanol and applying a drop of very dilute suspension on carbon-coated grids. For the reduced samples, all samples were reduced in H_2 in 573 K for 4 h.

TPR profiles were obtained on a Tianjin XQ TP 5080 auto adsorption apparatus. A 15-mg sample of the calcinated catalyst was outgassed at 473 K under Ar flow for 2 h. After the sample was cooled to room temperature under Ar flow, the in-line gas was switched to 5% H_2/Ar, and the sample was heated to 773 K at a ramping rate of 10 K·min^{-1}. The H_2 consumption was monitored by a TCD (thermal conductivity detector). The copper dispersion and the specific surface area of metallic copper (SA_{Cu}) of the catalysts were measured by dissociative N_2O adsorption.[28] The specific surface area of metallic copper is calculated from the amount of H_2 consumption 1.46×10^{19} with copper atoms per m^2.[29]

XPS experiments were carried out with a Perkin-Elmer PHI 5000C ESCA system equipped with a hemispherical electron energy analyzer. The Mg Kα (hν = 1253.6 eV) anode was operated at 14 kV and 20 mA. All binding energies are calibrated using the carbonaceous C 1s line at 284.6 eV as reference. The experimental errors are within ±0.2 eV.

2.3 Activity test

The catalytic activity test was performed using a fixed-bed microreactor. Typically, 0.6 g of catalyst (40-60 meshes) sample was loaded into a stainless steel tubular reactor with the thermocouple inserted into the catalyst bed for better control of the actual pretreatment and reaction temperature. Catalyst activation was performed at 573 K for 4 h with a ramping rate of 2 K·min^{-1} from room temperature under the 5% H_2/Ar (V/V) atmosphere. After cooling to the reaction temperature, 5 wt.% DMO (purity>99%) in methanol and H_2 were fed into the reactor at a H_2/DMO molar ratio of 100 and a system pressure of 2.5 MPa. The reaction temperature was first set at 493 K and LHSV of DMO ranged from 0.08 to 1.00 h^{-1}. For the TOF values calculation, the LHSV of DMO was set at 2.80 h^{-1} to control the initial conversion lower than 20%. The products were condensed, and analyzed on a gas chromatograph (Finnigan Trace GC ultra) fitted with an HP-5 capillary column and a flame ionization detector (FID).

All the catalysts are reduced at 573 K for 4 h under the 5% H_2/Ar (V/V) atmosphere prior to the catalytic test.

3. Results

3.1 Structural and textural properties

The physicochemical parameters of the respective catalysts are listed in Table 1. It is found that pure P25 possesses a BET specific surface area of 44.0 m^2·g^{-1}, and no obvious deviation from that value was observed in the Cu/P25 catalyst. We also find that, along with the variation in BET value, a similar trend of pore volume as well as pore diameter among the four catalysts were observed, consistent well with results from Au/P25 catalysts observed by Jovic and coworkers,[21] in which they also found a similar trend of physicochemical parameters variation, and they attributed the trends to sharply varied physicochemical properties of different titania supports. From the N_2 adsorption-desorption isotherm of the respective catalysts (Fig. S1, ESI†), all the catalyst samples exhibit Langmuir type IV isotherms, the H1-type hysteresis loop, corresponding to a typical large-pore mesoporous material.[14] Additionally, each sample displayed a significant N_2 adsorption-desorption hysteresis at high relative pressure of P/P_0>0.9, which serves as a sign of a high degree of textural porosity.[14] Notably, catalysts that enjoy similar S_{BET} data

Table 1 The textural properties and chemical compositions of the catalysts.

Sample	S_{BET}(m^{2}g^{-1})	V_{pore}(cm^{3}g^{-1})	D_{pore}(nm)	D_{Cu}[a](%)	SA_{Cu}[a](m^{2}g^{-1})	BE_{Cu}[b](eV)	BE_{Cu}[c](eV)	BE_{Ti}[b](eV)	BE_{Ti}[c](eV)	TOF[d](h^{-1})
P25	44.0	0.36	27.4	-	-	-	-	-	-	-
Cu/P25	49.0	0.35	28.7	28.3	38.3	933.8	933.0	460.8	459.8	9.1
Cu/M	45.6	0.19	12.6	17.8	24.1	933.9	932.8	460.5	459.1	0.59
Cu/A	42.7	0.24	12.5	19.5	26.3	933.8	932.9	461.0	459.0	0.46
Cu/R	24.6	0.11	3.76	11.3	15.3	934.0	933.0	459.5	459.0	8.0

[a] Cu dispersion (D_{Cu}) and Cu metal surface area (SA_{Cu}) determined by N_2O titration method. [b] Binding energy (Cu $2p_{3/2}$ and Ti $2p_{3/2}$) of catalysts calcinated at 823 K. [c] Binding energy (Cu $2p_{3/2}$ and Ti $2p_{3/2}$) of catalysts reduced at 573 K. [d] Reaction condition: P = 2.5 MPa, H_2/DMO = 100 mol/mol, and LHSV of DMO = 2.80 h^{-1}, T = 493 K.

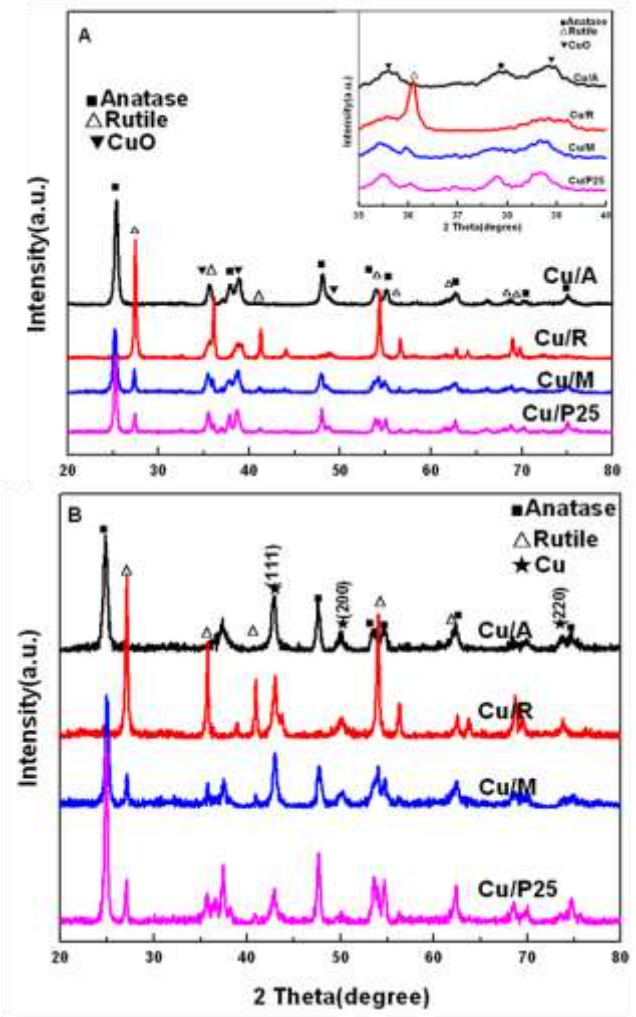

Fig. 1 XRD patterns of different catalysts (A) calcinated at 823 K (inset: magnified XRD image, 35~40°) and (B) reduced at 573 K.

show sharply different D_{Cu} and SA_{Cu} values, which should be ascribed to sharply varied interaction between copper species and supports: it is known that an intimate metal-support interaction leads to a high metal dispersion, while poor interaction would induce a poor dispersion, despite high specific areas of catalysts.

The XRD characterizations of such catalysts calcinated at 823 K are shown in Fig. 1A. It is unambiguous that all samples showed strong diffraction lines that respectively ascribed to anatase and rutile, pointing out that no obvious phase transformation occurred in the structural and textural properties of P25, pure anatase, rutile support and the mixture support. Relative weak diffraction peaks in the proximity of 35.5°, 38.7° and 48.7° characteristic of monoclinic CuO (JCPDS 48-1548) were observed for all of such catalysts, which indicates a slight aggregation of copper oxide species. XRD patterns of the respectively reduced Cu/TiO_2 catalysts are shown in Fig. 1B. It can be easily distinguished that upon reduction at 573 K, the peaks (2θ = 35.5°, 38.7°, 48.7°) of copper oxides for the calcinated samples disappeared, indicating a good reduction of CuO species. For the reduced ones, it is obvious to observe the appearance of the peaks (2θ = 43.5°, 50.4°, 74.1°) ascribed to Cu (111), Cu (200) and Cu (220) diffraction peaks (JCPDS 01-1241) and vividly, metallic copper diffraction line in the Cu/P25 is weaker than those in the other three, indicating a better dispersion of copper species, which confirms well with copper dispersion and SA_{Cu} data from N_2O titration data listed in Table 1.

As the TEM images of reduced catalysts in Fig. 2 showed, it is distinguishable that the P25 comprises of small spherical anatase crystallites, and larger angular rutile crystallites,[21] both of which were evident in the image. Previous research on Au/TiO_2 system indicates it is the active metal species preferentially located at the interface between anatase and rutile that act as a reactive center.[21] Here in the Fig. 2E, the HRTEM image of the reduced Cu/P25 catalyst illustrates the lattice fringes of 0.232 nm and 0.350 nm which fit well with the rutile (220) and anatase (101) planes respectively, confirming the coexistence of the anatase and rutile in the P25 supported system. The lattice fringe of 0.208 nm corresponding to the metallic Cu (111) planes in the interface of anatase and rutile reveals the successful synthesis of the P25 supported copper catalysts. As we know, the variation of interactions among cupreous species and support significantly influenced the stability and redox properties of the catalyst.[30] Similar observations were made by Tsukamoto,[31] Jovic[21] and Akita[32] for the Au/TiO_2 photocatalysts, whose work confirmed a preferentially location of Au nanoparticles at the interface between anatase and rutile titania. However, for the Cu/M, we observe no similar location at interfaces between such two kinds of titania after we counted even more than thirty images under different magnification, only to find mass amalgamation of copper species compared to the well dispersion of Cu in the Cu/P25. Analogously, for the Cu/A and Cu/R catalysts, we merely observed sintering and aggregation of copper species with no metals in the interface. TEM images under different magnification reveal similar results (Fig. S2, ESI†). From above discussion we can see that Cu/P25 displays better dispersion, conforming well with the XRD and N_2O titration results. Besides, the better dispersion as well as location at the interface may result from an intimate interaction between copper and the support.

3.2 Redox behaviour

TPR characterization is carried out to investigate the redox properties of the copper based catalysts. The results are shown in Fig. 3. It is distinguishable that a dominant peak at proximately

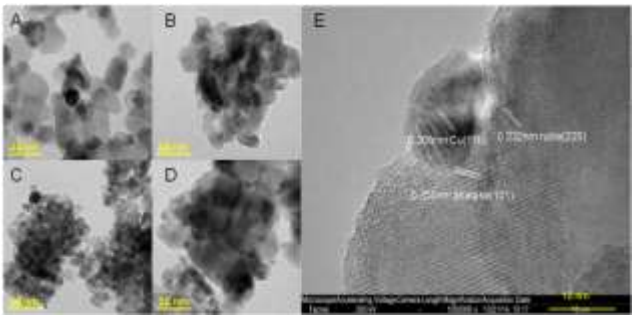

Fig. 2 TEM images for the reduced catalysts (A) Cu/P25; (B) Cu/M; (C) Cu/A; (D) Cu/R and (E) HRTEM of Cu/P25, all samples were pre-treated in H_2 at 573 K for 4 h.

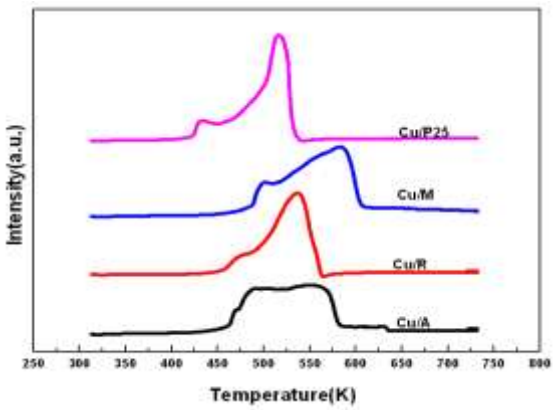

Fig. 3 TPR profiles of Cu/P25, Cu/M, Cu/R and Cu/A.

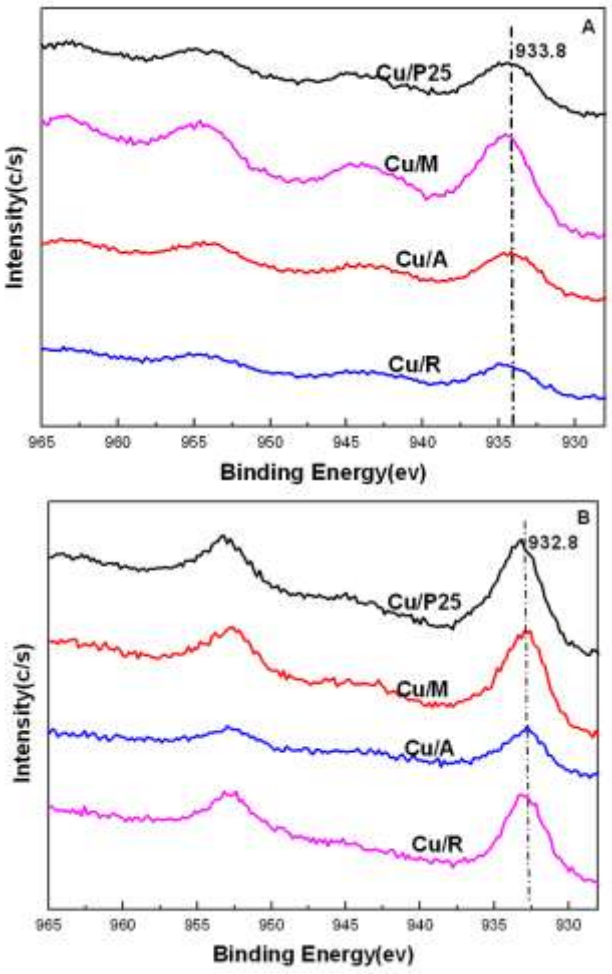

Fig. 4 Cu 2p XPS spectra of catalysts (A) calcinated at 823K and (B) reduced at 573K.

522 K with a shoulder peak at about 433 K can be picked out in Cu/P25, indicating a coexistence of two distinctive copper species, well dispersed and bulk ones. For the Cu/R and Cu/M catalysts, similar results can be obtained. However, in such catalysts of Cu/R and Cu/M we can find a higher reduction temperature compared to that of Cu/P25, which may imply higher reduction ability deriving from intimate interaction between copper and supports for the Cu/P25, in accordance to studies from Wen[33] and Vaudagna *et al*.,[34] who also observed an increased reduction of copper species enhanced by interaction between metal and supports. The result was also in great consistency with indication from TEM images that an intimate interaction would occur in the Cu/P25 system. Notably, for the Cu/A catalyst, broad peaks pertaining three distinct copper species occurred. We ascribe the three peaks as follows: the shoulder peak at about 468 K may be assigned to well-dispersed copper species, while 487 and 560 K should be assigned to copper oxide species better interacted with the support and bulk CuO particles. In a word, we come to a conclusion that compared to the other three catalysts, there is an intimate interaction between Cu and the support in the Cu/P25 catalyst, which may also accounts for a remarkable performance in activity test.

3.3 Chemical state and surface composition

The Cu 2p XPS results of the calcinated catalysts are shown in Table 1 and Fig. 4A, and the binding energy of Cu $2p_{3/2}$ peak in the proximity of 933.8 eV along with the presence of the characteristic shakeup satellite peaks suggests that the copper oxidation state is +2 in all the four catalysts.[14] Here we can clearly see that in Cu/TiO_2 catalysts there is a slightly higher binding energy for Cu $2p_{3/2}$ present compared with those of Cu/SiO_2 from literature,[35] indicating that compared to silica-supported system, a stronger interaction between the copper oxide and the titania supports occurred, which is highly consistent with observation by Wen[35] and Chen[36] *et al*. Fig. 4B shows the Cu 2p XPS spectra of the reduced catalysts, all of which were pre-treated in H_2 at 573 K for 4 h. The peak at approximately 932.8 eV has been assigned to metallic Cu^0 and/or Cu^+, as the binding energies of Cu^0 and Cu^+ are not distinguishable based on the Cu $2p_{3/2}$ peak.[37,38] Besides, the shakeup satellite peaks evident in the calcinated samples disappeared, which also verifies that most of the surface copper species in the catalysts are in the reduced state.[35] Admittedly, there is a wide weak peak between the 942~944eV for some reduced catalysts, indicating an existence of some Cu^{2+} species, which may stem from minor oxidation in the procedure of sample preparation or baseline oscillations in the XPS apparatus. However, based upon previous investigations, such peaks are too minute to affect the peak fitting results, and thus could be ignored.

From the Cu 2p XPS results, clear shifts of the binding energy can be observed in the reduced samples. It is found that Cu/P25 sample displays higher BE compared with other samples that show nearly same BE values of Cu 2p at 932.8 eV (see Fig. 4B). For the Ti 2p XPS profiles of the reduced samples in Fig. 5, it is interesting to observe clear chemical shift of the BE deriving reduction of Ti^{4+} to Ti^{3+} in the TiO_2 or the electron transfer from Cu to TiO_2. A clear BE shift of Ti 2p about 1.8 eV after reduction in both Cu/A and Cu/M, but this kind of BE shift value is negligible in the Cu/R. As Panpranot *et al.* has proved, Ti^{4+} in the

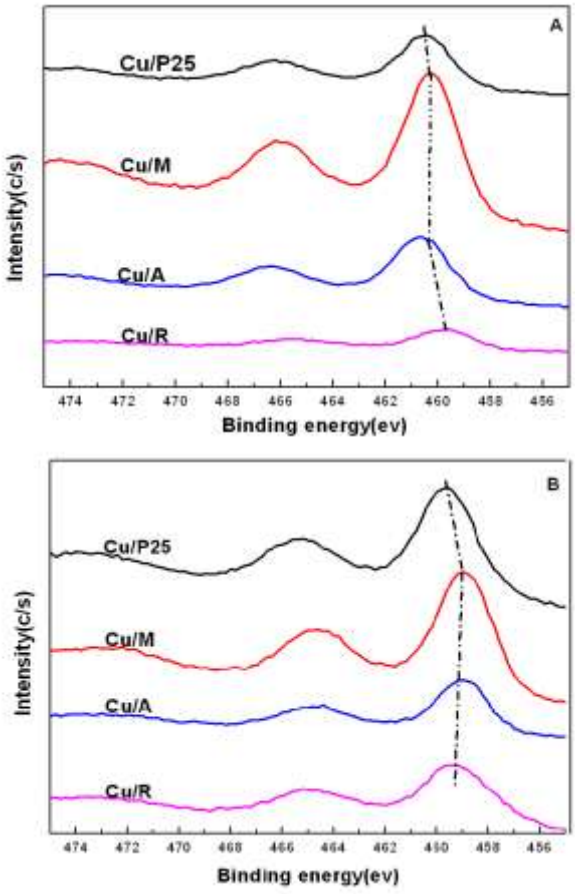

Fig. 5 Ti 2p XPS spectra of catalysts (A) calcinated at 823K and (B) reduced at 573K.

Table 2 Surface Cu component of catalysts reduced at 573 K based on Cu LMM deconvolution.

Sample	*KE(eV)*[a]		*AP(eV)*[b]		*$BE_{Cu2p3/2}$(eV)*[c]	*Cu^0/Cu^+*[d]
	Cu^+	Cu^0	Cu^+	Cu^0		
Cu/P25	916.0	918.6	1849.0	1851.6	933.0	0.857
Cu/M	916.2	919.1	1848.9	1851.8	932.7	1.021
Cu/A	916.1	918.8	1848.9	1851.6	932.8	0.932
Cu/R	916.0	918.9	1849.0	1851.9	933.0	0.904

[a] Kinetic energy; [b] Auger parameter; [c] Binding energy of the reduced samples; [d] $Cu^0/(Cu^+)\times 100\%$

rutile TiO_2 is more difficult to be reduced to Ti^{3+} because rutile is more thermodynamically and structurally stable than anatase,[39] conforming that there was almost no decline in the BEs of Ti 2p in Cu/R after reduction. Therefore, the greater BE shift in Cu/A and Cu/M are mainly ascribed to the reduction of Ti^{4+} to Ti^{3+} in the TiO_2. However, in the sample of Cu/P25, the Cu 2p shows higher BE value compared with other samples and the shift of Ti 2p to lower BE can also be observed, verifying that the electrons of Cu are transferred to the P25 support due to the preferential location at the interface. This observation was also evidenced in the Cu/TiO_2-SiO_2 catalysts by Wen's work.[35] In a word, preferential location of copper at interface between anatase and rutile is beneficial for electron transfer from Cu to P25 TiO_2, enhancing metal-support interaction and thus contributing to a higher activity of Cu/P25.

To further investigate the synergic effect between Cu^0 and Cu^+, the Cu LMM X-ray induced Auger spectra (XAES) was shown in Fig. S3 (ESI†). The presence of the kinetic energies of 916.6 and 918.5 eV strongly suggest the co-existence of the Cu^+ and Cu^0 species in the reduced catalysts.[14] Deconvolution of the original Cu LMM peaks was thus carried out and the peak positions as well as their contributions extracted from the deconvolution are listed in Table 2. As is shown in Table 2, the Auger parameter of copper kept around *ca*. 1851-1852 eV, suggesting the presence of Cu^+ species along with the metallic copper.[40] Also, the asymmetric Cu LMM peaks and the modified Auger parameter α' at *ca*. 1851.0 eV ascribed to Cu^0 and *ca.* 1849.0 eV ascribed to Cu^+ clearly verified the co-existence of the Cu^0 and Cu^+ species on the surface of the catalysts.[14] It seems that crystal phases greatly affected the distributions of surface Cu^+ and Cu^0, as the molar ratio of surface Cu^+/Cu^0 differed from each other in the samples. A higher amount of surface Cu^+ species was observed in the Cu/P25.

3.4 Catalytic activities and stability

To understand the origin of the catalytic reactivity over Cu/TiO_2 catalysts, we investigated the relationship between catalytic performance and intrinsic structure of catalysts with a probe reaction of the gas-phase hydrogenation of DMO by tuning the LHSV value.

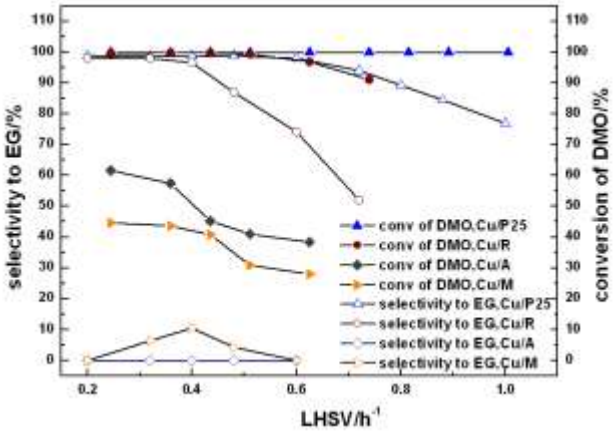

Fig. 6 Catalytic performance of the catalysts. Reaction condition: P = 2.5 MPa, T = 493 K, H_2/DMO = 100 (mol/mol).

Fig. 6 shows the conversion of DMO as well as the selectivity to EG over various catalysts. As is obviously exhibited, the Cu/P25 exerted an optimal catalytic activity, even at a high LHSV of 1.0 h^{-1}, whereas the other three deactivated markedly. For Cu/P25, a yield of *ca.* 98.9% was available under an optimized reaction condition. These results clearly demonstrate the high efficiency of the Cu/P25 catalyst in the selective hydrogenation of DMO to EG. The optimal catalytic performance of Cu/P25 may derive from a strong interaction between copper located at the interface and P25 in which lies a synergetic effect of anatase and rutile. This finding is also unambiguously stated in HRTEM and deduced from TPR profiles. From the physicochemical properties we also find that the Cu/P25 catalyst owns the largest BET area and SA_{Cu} as well as copper dispersion. Combining such observations with TEM and TPR results, we come to a conclusion that the interaction between Cu and P25 induces a better dispersion as well as an optimized Cu^0/Cu^+ distributions, which cooperate to exert a better catalytic performance. P25 supported catalyst is expected to be capable of increasing the amount of copper species with partial positive charges resulting from a better metal support interaction as well as electron transfer between copper and P25 titania. Similar electron transfer was observed by Jovic[21] and Tsukamoto[31] in the Au/TiO_2 system.

To gain further insights into the crystalline effect of TiO_2 supports, the TOF values were investigated to compare the catalytic performance of the catalyst based on the moles of DMO converted on per mole of surface sites per hour (see Table 1). It is unambiguous that Cu/P25 exhibited a highest TOF value of 9.1 h^{-1}, which is 13.8% higher than that of Cu/R and more than 10 times larger than those of Cu/A and Cu/M.

For a deeper investigation of the synthesized catalysts, we also conducted test of long-term catalytic performance (Fig. S4, ESI†) at 493 K with a LHSV of 0.3 h^{-1}. During the reaction process, we discovered no obvious deactivation of Cu/P25 even after a long period of 96 h occurred, and the yield to EG remained in the proximity of 95%, indicating that a long-term catalytic life span of the P25 supported copper-based catalyst, which was also ascribed to an intimate interaction between the Cu species and P25 support.

To exclude the effects of titania supports in catalytic performance of DMO hydrogenation to EG, we applied pure P25 as a catalyst into the hydrogenation of dimethyl oxalate, only to find too slight DMO conversion (less than 1.0%, reaction condition identical to that of stability test (Fig. S1, ESI†)). Thus, the effect of titania support could be neglected.

4. Discussion

Although copper-based catalysts for hydrogenation or

hydrogenolysis were extensively studied and various supports such as Al_2O_3, ZrO_2, SiO_2, and hydroxyapatite have been adopted to modify their catalytic performance, [2,4,41,42] reports related to titania-supported copper catalysts in ester hydrogenation remain scarce. In our present study, an outstanding hydrogenation activity could be achieved via the Cu/P25 catalyst. Structural and textural evaluation presented the highest BET area and SA_{Cu}, while the redox behaviour indicates a better metal-support interaction of CuP25, compared to the other three catalysts. Notably, a highest dispersion and the greatest quantity of surface Cu^+ species were also observed in the Cu/P25, as determined by N_2O adsorption and XAES.

The subtle information on catalytic activities for catalysts is indicated by TOF values, among which Cu/P25 displayed a highest one of 9.1 h^{-1} (see Table 1), suggesting a great effect of titania crystal phase in catalytic system for DMO hydrogenation. Although there seems no obvious variation in physicochemical factor such as S_{BET}, D_{pore} and V_{pore}, TOF values differ sharply and a superiority of Cu/P25 could be observed.

Numerous work has been conducted to investigate the catalytic role of Cu^+ and Cu^0 in ester hydrogenation.[8,14,41,42] Poels *et al.* suggest that Cu^0 sites dissociatively absorb hydrogen molecules and that Cu^+ sites strongly bind and activate the ester and acyl groups.[43] Dai's group observed Cu^+ may function as electrophilic or Lewis acid sites to polarize the C=O bond via the electron lone pair on oxygen, thus improving the reactivity of the ester group in DMO,[14] while Gong *et al*. revealed a cooperative effect between surface Cu^0 and Cu^+ as well as a proper Cu^0/Cu^+ ratio in the Cu based catalysts,[41] which was verified by He and coworkers.[42] Accordingly, the efficiency of DMO hydrogenation to EG may greatly rely on the synergy of Cu^0 and Cu^+ sites on the catalyst surface and an optimized Cu^0/Cu^+ distributions may exist to exert a high activity. In our present work, a highest amount of surface Cu^+ species was observed in the Cu/P25 which presents highest yield to EG. However, this result does not apply to all cases. As is revealed, in the Cu/P25 catalyst, P25 supported catalyst is expected to be capable of increasing the amount of copper species with partial positive charges resulting from a better metal support interaction as well as electron transfer, while no similar behavior occurred for the other catalysts, which may account for a highest Cu^+ in specific Cu/P25 system. Similar result was observed by He *et al.* in the CuB/SiO_2 system, and they ascribed it to greater acidity and electron affinity of boric oxide.[42]

We also note that copper dispersion and specific surface area of metallic copper play a significant role in the catalytic performance, which has been confirmed by various investigations.[8,30,35,42] It is distinguishable that the highest SA_{Cu} was achieved in the Cu/P25 catalyst, which results from a better dispersion of copper species on the support. Also, from the TEM images, we can clearly see a better dispersion of copper species in the Cu/P25, while the HRTEM images indisputably showed us a location of active copper at the interface between anatase and rutile titania, indicating an intimate interaction between Cu and support in the Cu/P25 catalyst, which may be responsible for the optimized catalytic activity. In short, a strong interaction between Cu and P25 support greatly helps with the dispersion of metallic copper, which also contributes to the higher catalytic activity and stability.

5. Conclusions

In summary, a series of copper based titania supported catalysts were synthesized for the display of an optimized catalytic performance. The crystalline phases of TiO_2 play a consequential role in the activity for the vapor-phase hydrogenation of DMO to EG, as it influences the interaction between copper and the support, hence affecting the metallic dispersion of copper and the ratio of active Cu^0/Cu^+. The P25 supported copper catalyst exerts the excellent catalytic performance because of an intimate interaction between copper and P25 support occurred. This interaction was validated by the location of Cu at the interface between anatase and rutile, enhancing the copper dispersion and inducing an optimized Cu^0/Cu^+ distribution.

Acknowledgements

We thank financial support by the Major State Basic Resource Development Program (Grant No. 2012CB224804), Natural Science Foundation of China (Project 21373054, 21173052), the Natural Science Foundation of Shanghai Science and Technology Committee (08DZ2270500).

Notes and references

[a]*Department of Chemistry and Shanghai Key Laboratory of Molecular Catalysis and Innovative Materials, Fudan University, Shanghai 200433,P. R. China. Fax: (+86–21) 55665701; Tel: (+86–21) 55664678; E-mail:wldai@fudan.edu.cn*

† Electronic Supplementary Information (ESI) available: [details of any supplementary information available should be included here]. See DOI: 10.1039/b000000x/

‡ Footnotes should appear here. These might include comments relevant to but not central to the matter under discussion, limited experimental and spectral data, and crystallographic data.

1 H. Yue, Y. Zhao, X. Ma and J. Gong, *Chem. Soc. Rev*., 2012, **41**, 4218.
2 C. Wen, Y. Cui, W. L. Dai, S. Xie and K. N. Fan, *Chem. Commun*., 2013, **49**, 5195.
3 S. Wang, X. Li, Q. Yin, L. Zhu and Z. Luo, *Cata. Commun*., 2011, **12**, 1246.
4 C. Wen, Y. Cui, X. Chen, B. Zong and W. L. Dai, *Appl. Catal. B*, 2015, **12**, 483.
5 L. Zhao, Y. Zhao, S. Wang, H. Yue, B. Wang, J. Lv and X. Ma, *Ind. Eng. Chem. Res*., 2012, **51**, 13935.
6 J. Lin, X. Zhao, Y. Cui, H. Zhang and D. Liao, *Chem. Commun.*, 2012, **48**, 1177.
7 C. Wen, Y. Cui, A. Y. Yin, K. N. Fan and W. L. Dai, *ChemCatChem*, 2013, **5**, 138.
8 L. Chen, P. J. Guo, M. H. Qiao, S. R. Yan, H. X. Li, W. Shen, H. L. Xu and K. N. Fan, *J. Catal*., 2008, **257**, 172.
9 A. Y. Yin, X. Y. Guo, W. L. Dai, H. X. Li and K. N. Fan, *Appl. Catal. A*, 2008, **349**, 91.
10 A. Y. Yin, C. Wen, W. L. Dai and K. N. Fan, *Appl. Surf. Sci.*, 2011, **257**, 5844.
11 A. Y. Yin, X. Y. Guo, W.L. Dai and K. N. Fan, *J. Phys. Chem. C*, 2010, **114**, 8523.
12 A. Y. Yin, J. W. Qu, X. Y. Guo, W. L. Dai and K. N. Fan, *Appl. Catal. A*, 2011, **257**, 39.
13 A. Y. Yin, C. Wen, X. Y. Guo, W. L. Dai and K. N. Fan, *J. Catal.*, 2011, **280**, 77.
14 A. Y. Yin, X. Y. Guo, W. L. Dai and K. N. Fan, *J. Phys. Chem. C*, 2009, **113**, 11003.
15 C. Yogi, K. Kojima, T. Hashishin, N. Wada, Y. Inada, E. D. Gaspera, M. Bersani, A. Martucci, L. Liu and T. K. Sham, *J. Phys. Chem. C*, 2011, **115**, 6554.
16 N. M. Dimitrijevic, B. K. Vijayan, O. G. Poluektov, T. Rajh, K. A. Gray, H. He and P. Zapol, *J. Am. Chem. Soc.*, 2011, **133**, 3964.
17 S. M. Chang, Y. Y. Hsu and T. S. Chan, *J. Phys. Chem. C*, 2011, **115**, 2005.
18 B. Xia, S. Ding, H. Wu, X. Wang and X. Wen, *RSC Adv.*, 2012, **2**, 792.
19 Z. Z. Jiang, Z. B. Wang, Y. Y. Chu, D. M. Gu and G. P. Yin, *Energy Environ. Sci.*, 2011, **4**, 2558.
20 R. Kou, Y. Shao, D. Mei, Z. Nie, D. Wang, C. Wang,V. V. Viswanathan, S. Park, I. A. Aksay, Y. Lin, Y. Wang and J. Liu, *J. Am. Chem. Soc.*, 2011, **133**, 2541.
21 V. Jovic, W. T. Chen, D. X. Sun, M. G. Blackford, H. Idriss and I. N. Waterhouse, *J. Catal.*, 2013, **305**, 307.
22 M. Murdoch, G. I. N. Waterhouse, M. A. Nadeem, J. B. Metson, M. A. Keane, R. F. Howe, J. Llorca and H. Idriss, *Nat. Chem.*, 2011, **3**, 489

23 R. Katoh, M. Mural and A. Furube, *Chem. Phys. Lett.*, 2008, **461**, 238.
24 K. M. Shindler and M. Kunst, *J. Phys. Chem.*, 1990, **94**, 8222.
25 A. Yamakata, T. A. Ishibashi, H. Onishi, *Chem. Phys.*, 2007, **339**, 133.
26 K. Y. Ho and K. L. Yeung, *Gold Bull.*, 2007, **40**, 15.
27 F. Liao, Y. Huang, J. Ge, W. Zheng, K. Tedsree, and P. Collier, X. Hong and S. C. Tsang, *Angew. Chem. Int. Ed.*, 2011, **50**, 2162.
28 Z. Y. Pu, X. S. Liu, A. P. Jia, Y. L. Xie, J. Q. Lu and M. F. Luo, *J. Phys. Chem. C*, 2008, **122**, 15045.
29 C. Chinchen, C. M. Hay, H. D. Vandervell, K. C. Waugh, *J. Catal.*, 1987, **103**, 79.
30 S. Zhao, H. R. Yue, Y. J. Zhao, B. Wang, Y. C. Geng, J. Lv, S. P. Wang, J. L. Gong and X.B. Ma, *J. Catal.*, 2013, **297**, 142.
31 D. Tsukamoto, Y. Shiraishi, Y. Sugano, S. Ichikawa, S. Tanaka, and T. Hirai, *J. Am. Chem. Soc.*, 2012, **134**, 6309.
32 T. Akita, P. Lu, S. Ichikawa, K. Tanaka and M. Haruta, *Surf. Interface Anal.*, 2001, **31**, 73.
33 C. Wen, F. Li, Y. Cui, W. L. Dai and K. N. Fan, *Catal. Today*, 2014, **223**, 117.
34 S. R. Vaudagna, S. A. Canavese, R. A. Comelli, N. S. Fı'goli, *Appl. Catal. A*, 1998, **168**, 39.
35 C. Wen, A. Y. Yin, Y. Cui, X. Yang, W. L. Dai and K. N. Fan, *Appl. Catal. A*, 2013, **458**, 82.
36 C. S. Chen, T. C. Chen, C. C. Chen, Y. T. Lai, J. H. You, T. M. Chou, C. H. Chen and J. F. Lee, *Langmuir*, 2012, **28**, 9996.
37 F. Severino, J. L. Brito, J. Laine, J. L. G. Fierro, A. L. Agudo, *J. Catal.*, 1998, **177**, 82.
38 S. Velu, K. Suzuki, M. Vijayaraj, S. Barman, C. S. Gopinath, *Appl. Catal. B*, 2005, **55**, 287.
39 J. Panpranot, K. Kontapakdee, P. Praserthdam, *Appl. Catal. A*, 2006, **314**, 128.
40 W. L. Dai, Q. Sun, J. F. Deng, D. Wu, Y. H. Sun, *Appl. Surf. Sci.*, 2001, **177**, 172.
41 J. Gong, H. Yue, Y. Zhao, S. Zhao, L. Zhao, J. Lv, S. Wang and X. Ma, *J. Am. Chem. Soc.*, 2012, **134**, 13922.
42 Z. He, H. Lin, P. He, Y. Yuan, *J. Catal.*, 2011, **277**, 54.
43 E. K. Poels and D. S. Brands, *Appl. Catal. A*, 2000, **191**, 83.

Remarkable crystal phase effect of Cu/TiO_2 catalysts in the selective hydrogenation of dimethyl oxalate

Bin Wang, [a] Chao Wen, [a] Yuanyuan Cui, [a] Xi Chen, [a] and Wei-Lin Dai [*a]

[a] Department of Chemistry and Shanghai Key Laboratory of Molecular Catalysis and Innovative Materials, Fudan University, Shanghai 200433, P. R. China

The crystal phase of titania support plays a significant role in catalytic performance for the hydrogenation of dimethyl oxalate. A higher catalytic performance as well as stability could be achieved for the Cu/P25, due to a synergy of highly dispersed copper species and appropriate Cu^0/Cu^+ ratio on the surface, which stem from an intimate interaction between copper and P25 support.